

SPATIAL- AND TIME-DEPENDENT THERMAL AND ELECTRICAL BEHAVIOR
OF QUENCHING HIGH-TEMPERATURE SUPERCONDUCTING COMPOSITE
TAPES

by
Mamoon I. Yunus

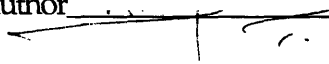
B.S.M.E., Georgia Institute of Technology
(1991)
M.S.M.E, Massachusetts Institute of Technology
(1993)

Submitted to the Department of Mechanical Engineering
in Partial Fulfillment of the Requirements for the Degree of

MECHANICAL ENGINEER'S DEGREE
at the
MASSACHUSETTS INSTITUTE OF TECHNOLOGY
July 1995

© Massachusetts Institute of Technology 1995. All rights reserved.

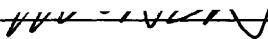
Signature of Author



Department of Mechanical Engineering
July 10, 1995



Certified by



Yukikazu Iwasa
Thesis Supervisor



Accepted by



Ain A. Sonin
Chairman, Departmental Graduate Committee

MASSACHUSETTS INSTITUTE
OF TECHNOLOGY

SEP 21 1995

Barker Eng

LIBRARIES

SPATIAL- AND TIME-DEPENDENT THERMAL AND ELECTRICAL BEHAVIOR OF QUENCHING HIGH-TEMPERATURE SUPERCONDUCTING COMPOSITE TAPES

by

Mamoon I. Yunus

Submitted to the Department of Mechanical Engineering on July 10, 1995,
in Partial Fulfillment of the Requirements for the Degree of
Mechanical Engineer's Degree
at the Massachusetts Institute of Technology

Abstract

An experimental and analytical study of the thermal and electrical behavior of a quenching silver-sheathed BSCCO-2223 tape is presented. Both spatial and temporal characteristics of the quenching tape are examined in detail for a quench induced with a current pulse applied over a heater located at the midpoint of the tape. The sample tested has a spatially nonuniform critical current distribution. This nonuniformity in the critical current results in asymmetric spatial temperature profiles with the section of lowest critical current showing the largest temperature rise. Experimental results, obtained for transport current of 55 A and operating temperature of 60 K in zero magnetic field, agree well with those based on theory.

Thesis Supervisor: Dr. Yukikazu Iwasa

Title: Research Professor, Francis Bitter National Magnet Laboratory, and Senior Research Engineer,
Department of Mechanical Engineering, MIT.

Acknowledgements

My four years of graduate work at the Francis Bitter National Magnet Laboratory, MIT have been the most exciting years of my life. I want to thank Dr. Yuki Iwasa for his financial, academic, and personal support during my years at MIT. I also want to thank John Williams for his on-the-fly corridor discussions. Dave Johnson and Mel Vestal were pivotal in developing my hands-on technical skills. I thank them for their patience.

I am grateful to Hunwook Lim, and Jun Kim for their help and company. Sharing office space with them created a mutually beneficial environment.

I would like to acknowledge Sumitomo Electric and Intermagnetic General Corporation for providing the high- T_c tapes.

Finally, I want to thank my wife and my parents for their unconditional support.

Table of Contents

Abstract.....	2
Acknowledgements.....	3
Table of Contents.....	4
List of Figures.....	6
Nomenclature.....	7
1 Introduction.....	9
1.1 The HTS Era.....	9
1.2 Thesis Outline.....	10
2 Quenching in HTS tapes.....	11
2.1 1-D Analytical Model of Composite Tapes.....	11
2.2 Current Sharing and Joule Heating.....	13
3 Experimental Technique and Results.....	16
3.1 Experimental Setup.....	16
3.2 Critical Current Measurement.....	18

3.3	Quench Initiation and Normal-Zone Propagation.....	19
3.4	Temperature Profiles.....	23
3.5	Verification of Temperature Measurement.....	23
4	Computer Simulation of Quenching.....	28
4.1	Simulation Algorithm.....	28
4.2	Finite Difference Method and Stability.....	28
4.3	Comparison of Results, Simulation and Experiment.....	30
4.3.1	Simulation with Nonuniform Critical Current Distribution.....	30
4.3.2	Simulation with Uniform Critical Current Distribution.....	31
4.4	Limitations of Simulation Code.....	34
5	Conclusions.....	35
5.1	Effect of Weak-Spots in Conductor.....	35
5.2	Protection Schemes for HTS Magnets.....	36
	References.....	38
	Appendix A.....	39

List of Figures

2.1	Section of a high- T_c superconducting tape with coordinate z along the conductor axis.....	12
2.2	Critical Current of a composite superconductor as a function of temperature for a given magnetic field. The conductor carries a constant transport current, I_t	13
3.1	Drawing of a silver-sheathed BSSCO tape positioned in a copper block.....	17
3.2	Locations of the voltage taps and the thermocouples on the BSSCO tape.....	18
3.3	E - field traces for the seven zones at $T_{op} = 60$ K.....	20
3.4	$I_c(T)$ for seven zones with $E_c = 1$ μ V criterion.....	21
3.5	$I_{cs}(T)$ for seven zones with $E_c = 25$ μ V criterion.....	22
3.6	$T(t)$ traces during quenching for $I_t = 55$ A and $T_{op} = 60$ K.....	25
3.7	$T(z,t)$ traces during quenching for $I_t = 55$ A and $T_{op} = 60$ K.....	26
3.8	$V(t)$ traces during quenching for $I_t = 55$ A and $T_{op} = 60$ K. Solid lines are measured; dotted lines are computed from the temperature traces shown in Figure 3.6.....	27
4.1	$T(z,t)$ profiles during quenching for $I_t = 55$ A and $T_{op} = 60$ K. Dotted lines are simulated profiles with nonuniform critical currents across the tape.....	32
4.2	$T(z,t)$ profiles during quenching for $I_t = 55$ A and $T_{op} = 60$ K. Dotted lines are simulated profiles with uniform critical current assumed across the entire tape.....	33

Nomenclature

A_{cd}	Conductor cross-sectional area	(cm ²)
A_m	Matrix cross-sectional area	(cm ²)
C_{cd}	Conductor volumetric specific heat	(J/cm ³ -K)
C_m	Matrix volumetric specific heat	(J/cm ³ -K)
C_{sc}	Superconductor volumetric specific heat	(J/cm ³ -K)
dz	Differential spatial element	(cm)
E	Electric field	(V/cm)
f	Volume or area fraction	(-)
g	Joule heating density	(W/cm ³)
I_c	Critical current	(A)
I_m	Matrix current	(A)
I_{sc}	Superconductor current	(A)
I_t	Transport current	(A)
I_{cs}	Critical sharing current	(A)
k_{cd}	Conductor thermal conductivity	(W/cm-K)
k_m	Matrix thermal conductivity	(W/cm-K)
k_{sc}	Superconductor thermal conductivity	(W/cm-K)
l	tape section length	(cm)
R_m	Matrix resistance	(Ω)
ρ_m	Matrix resistivity	($\mu\Omega\text{cm}$)
t	Time	(s)
T	Temperature	(K)

T_c	Critical temperature	(K)
T_{op}	Operating temperature	(K)
V	Voltage	(V)
z	Spatial coordinate	(cm)

1 Introduction

1.1 The HTS Era

January 27, 1986 marks the advent of a new era in superconducting technology. On that day, Karl Alex Müller and Johann Georg Bednorz synthesized a compound of barium, lanthanum, copper, and oxygen –a superconductor with the highest critical temperature (35 K) at that time. Their publication, “Possible high T_c superconductivity in the Ba-La-Cu-O system,” triggered an intense search for materials that would be superconducting at even higher temperatures. One year after Müller and Bednorz’s Nobel Prize-winning discovery, Paul Chu and Maw-Kuen Wu were the first to demonstrate that $\text{YBa}_2\text{Cu}_3\text{O}_7$ had a critical temperature of 95 K. This material is superconducting in liquid nitrogen which has a boiling point of 77 K. The use of liquid nitrogen, an inexpensive and easily available cryogenic coolant, for high- T_c superconductors (HTS) meant that the commercial applications of superconductivity would become economically feasible.

Since the discovery of the bismuth-based superconductors, a number of companies, led by Sumitomo Electric, and Intermagnetic General Corporation (IGC), have fabricated silver-sheathed $(\text{BiPb})_2\text{Sr}_2\text{Ca}_2\text{Cu}_3\text{O}_x$, commonly known as BSCCO-2223, tapes. Since the early 1990s, HTS tapes of lengths greater than ~ 10 cm have become available. Recently, HTS magnets have been developed and successfully tested at temperatures ranging from 4.2 - 77 K with background magnetic fields up to 22.5 T [1,2].

A superconductor is defined by three bounding parameters, a critical temperature, T_c , a critical current density, J_c , and a critical magnetic induction B_c . These three parameters form the critical surface of a superconductor. If all of the operating parameters of the superconductor, T , J , and B are confined within the critical surface, the material is superconducting. If the operating point crosses over the critical surface, the material transitions from the superconducting state to a resistive state. This transition is called a quench. This thesis presents an experimental and analytical study of the quenching process of silver-sheathed BSCCO tapes.

1.2 Thesis Outline

Chapter 2 presents a one-dimensional (1-D) analytical model of HTS tapes. The basic governing equations are presented. The current sharing phenomenon, observed in composite tapes is also explained. Current sharing has a significant effect on the quenching behavior of HTS tapes. Chapter 3 explains the experimental technique used to study the quenching process in HTS tapes. Results from the experiments are also presented in this chapter. Chapter 4 describes the simulation code used to predict the behavior of HTS tapes and a comparison of the analytical results with the experimental results. Chapter 5 presents conclusions, emphasizing the impact of this research on understanding the electrical and the thermal behavior of HTS tapes undergoing quench and on the development of protection schemes for HTS magnet systems.

2 Quenching in HTS Tapes

2.1 1-D Analytical Model of Composite Tapes

Figure 2.1 shows a section of an HTS tape simplified to one spatial dimension, z , which is set along the conductor axis. The temperature, $T(z,t)$ at any location, z , along the conductor axis, and for any time, t , can be obtained by solving the following power density equation [3]:

$$C_{cd}(T) \frac{\partial T}{\partial t} = \frac{\partial}{\partial z} \left(k_{cd}(T) \frac{\partial T}{\partial z} \right) + g_j \quad (2.1)$$

$C_{cd}(T)$ is the temperature-dependent composite tape's heat capacity, $k_{cd}(T)$ is the composite thermal conductivity, and g_j is the joule heating density which will be described in detail in the next section.

The material properties $C_{cd}(T)$ and $k_{cd}(T)$ are volumetrically averaged over the entire tape. The expressions for these two material properties are the following:

$$C_{cd}(T) = f C_m(T) + (1-f) C_{sc}(T) \quad (2.2)$$

$$k_{cd}(T) = f k_m(T) + (1-f) k_{sc}(T) \quad (2.3)$$

where the subscripts cd , m and sc represent the composite tape, silver sheath, and the BSCCO superconductor respectively. f is the volumetric fraction of the silver matrix in the tape. For a given conductor length, $f = A_m/A$ where A_m is the cross sectional area of the silver sheath and A is the total cross sectional area of the tape.

Since the material properties are temperature dependent, Equation 2.1 is a 1-D nonlinear partial differential equation which has to be solved numerically. The numerical solution of this equation is described in Chapter 4. To understand the Joule heating density term, g_j , in Equation 2.1 the current sharing phenomenon is described in the following section.

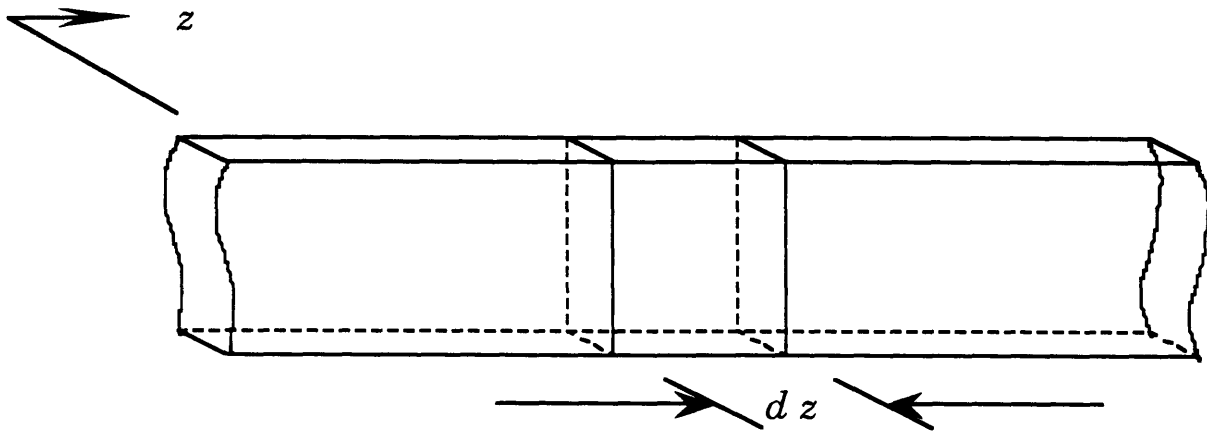


Figure 2.1: Section of a high- T_c superconducting tape with coordinate z along the conductor axis.

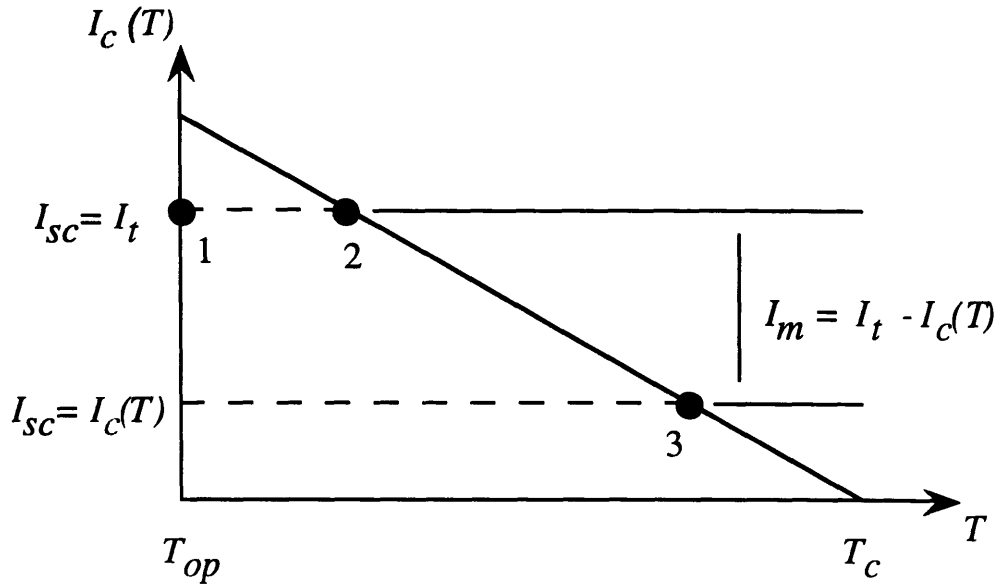


Figure 2.2: Critical Current of a composite superconductor as a function of temperature for a given magnetic field. The conductor carries a constant transport current, I_t .

2.2 Current Sharing and Joule Heating

When a section of the superconductor is heated and its temperature is raised, the transport current shifts from the superconductor to the silver sheath. In regions of such current shifts, current sharing occurs, such that current flows in both the superconductor and the silver matrix. Figure 2.2 shows a line approximation of the critical current of a superconductor, I_c , as a function of temperature, T for a given magnetic field. At point 1, with an operating temperature of T_{op} , the conductor is fully superconducting and all the transport current, I_t , flows through the superconductor ($I_{sc}=I_t$). As the temperature of the superconducting composite is increased from T_{op} , till point 2 the superconductor still carries all the

transport current. After point 2, an increase in the temperature of the conductor shifts part of the transport current to the silver matrix. Thus, at point 3, the superconductor now carries a lower current than point 2, and the matrix takes up the difference between the transport current and the current carried by the superconductor. This current carried by the matrix is represented by I_m . If the temperature of the composite conductor is increased beyond the critical temperature of the superconductor, T_c , then all of the transport current is carried by the silver matrix.

The Joule heating density for composite conductor is simply the product of the transport current and the voltage divided by the volume of the conductor:

$$g_j (T) = \frac{V I_t}{A_{cd} l} \quad (2.4)$$

where V is the voltage across the conductor, I_t is the transport current, A_{cd} is the cross sectional area of the composite conductor and l is the length of the conductor across which the voltage appears. The voltage can be computed by multiplying the matrix current, I_m , by the matrix resistance, R_m , of the length, l , of the composite conductor.

$$g_j (T) = \frac{I_m R_m I_t}{A_{cd} l} = \frac{[I_t - I_c(T)] \rho_m(T) I_t}{A_{cd} A_m} \quad (2.5)$$

where A_m is the cross sectional area of the silver matrix and $\rho_m(T)$ is the resistivity of the matrix.

Equation 2.5 is the most general form of the generation density. If all of the transport current flows

through the matrix then $I_c(T \geq T_c) = 0$ for Equation 2.5 and the composite conductor is fully normal. $g_j = 0$ if the temperature and the transport current of the composite tape lie within the $I_c(T)$ line of the superconductor as shown in Figure 2.2.

Substituting Equation 2.5 in Equation 2.1 gives the following modified power density equation for HTS composite tapes:

$$C_{cd}(T) \frac{\partial T}{\partial t} = \frac{\partial}{\partial z} \left(k_{cd}(T) \frac{\partial T}{\partial z} \right) + \frac{[I_t - I_c(T)] \rho_m(T) I_t}{A_{cd} A_m} \quad (2.6)$$

Equation 2.6 is the governing nonlinear partial differential equation (PDE) for the quenching process in HTS tapes. The numerical solution of this equation is described in Chapter 4.

3 Experimental Technique and Results

3.1 Experimental Setup

Figure 3.1 shows a silver-sheathed BSCCO test tape ~ 300 mm long placed in a narrow groove machined in a copper block. The bottom extension of the copper block is attached to the cold-head of a cryocooler. As shown in the figure, thermocouples and voltage taps are attached to the tape along its ~ 285° arc. A stainless steel heater, 25 mm in length, is located at the midpoint of the arc. Figure 3.2 shows the exact locations of the thermocouples and voltage taps along the test sample.

Type E thermocouples (Chromel vs. Constantan) were chosen for temperature measurement. Appendix A shows the thermoelectric voltage versus temperature, and the Seebeck Coefficient versus temperature (which indicates sensitivity) for a Type E thermocouple.

The thermocouples and voltage taps are attached to the tape with silver epoxy manufactured by Tra-Con, Incorporated. The use of silver epoxy--a poor electrical conductor--is necessitated because of the presence of transport currents. In previous experiments, low temperature Indium solder was used for attaching the thermocouples and the voltage taps to the sample. This method resulted in thermal damage to the tape, therefore silver epoxy was used instead. The reference junctions of the thermocouples are attached to the copper block. When the cryocooler is set at desired temperature, e.g. 60 K, all the thermocouples and their junctions are at 60 K. The thermoelectric voltage is zero. An increase in the temperature of the tape results in an increase in the voltage which is converted to temperature through the calibration data shown in Appendix A.

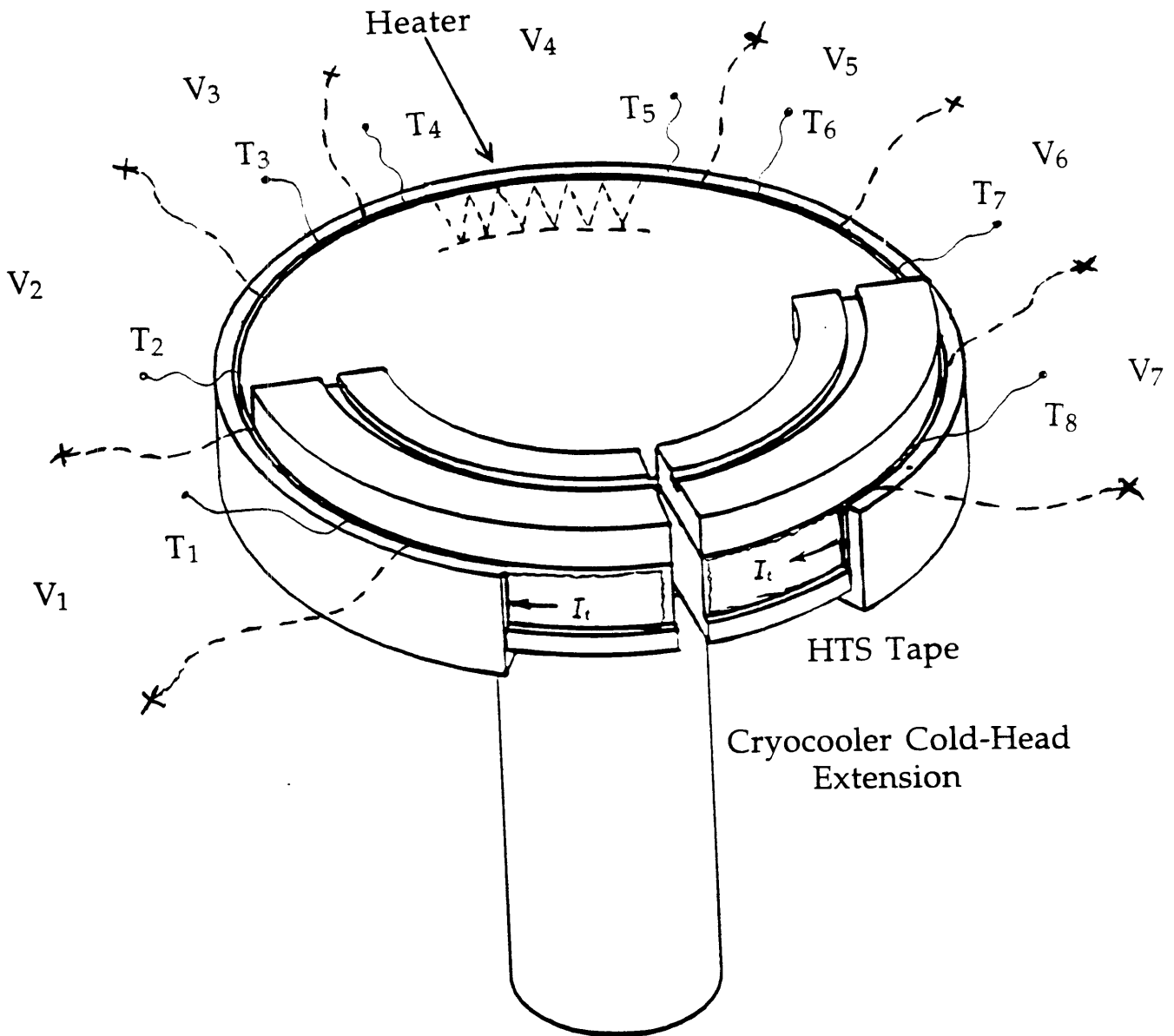


Figure 3.1: Drawing of a silver-sheathed BSSCO tape positioned in a copper block and maintained at T_{op} .

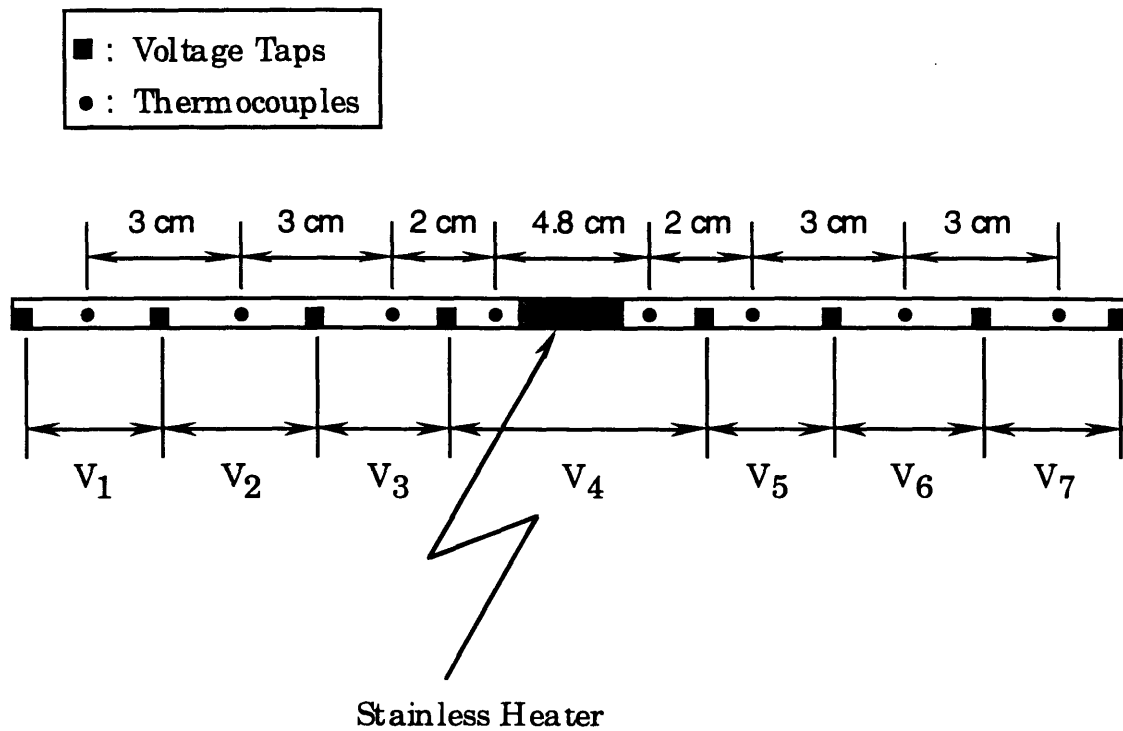


Figure 3.2: Locations of the voltage taps and the thermocouples on the BSSCO tape.

3.2 Critical Current Measurement

Initial experiments at given operating temperatures, T_{op} , revealed quench-induced temperature profiles that were asymmetric with respect to the heater location. Therefore, critical currents for the seven zones were obtained at operating temperatures between 40 ~ 80 K. The E vs I traces for $T_{op} = 60$ K, shown in Figure 3.3, reveals a significant variation in I_c among the seven zones. In particular, zones 5, 6 and 7 carry larger currents than the zones 1, 2, and 3. For a critical E -field, $E_c = 1 \mu\text{V}/\text{cm}$, the $I_c(T)$ plots are shown in Figure 3.4. The variation in $I_c(T)$ were most likely caused because of the variations inherent in the manufacturing process for the HTS tapes. Even for T_c values, manufactures report values between 93 ~ 110 K.

In addition to the variation in the I_c values for various zones, differences in the transition regions were observed. Large transition regions are observed in each of the traces. The large transition regions occur because of low index, n , values. The transition region is particularly large for zone 4. Temperature measurements for this critical current test indicate that each zone remains at the operating temperature, T_{op} , during the transition up to an E - field of $\sim 25 \mu\text{V}/\text{cm}$. Therefore, to account for the variation in the index-number, n , for the seven zones, a new critical current, "critical sharing current," $I_{cs}(T)$ is defined such that for $E_{cs} = 25 \mu\text{V}/\text{cm}$, the index-induced power generation can be neglected [4]. The $I_{cs}(T)$ plots based on this criterion are shown in Figure 3.5. In the simulation presented in Chapter 4, $I_{cs}(T)$ based on $E_c = 25 \mu\text{V}/\text{cm}$ is used to characterize the critical current line for each of the zones such that for $I_t \leq I_{cs}(T_{op})$, the current through the silver matrix $I_m \approx 0$ and $I_m \approx I_t - I_{cs}(T_{op})$ for $I_t \geq I_{cs}(T_{op})$.

The critical current measurements for the sample show that zones 1, 2, and 3 have lower critical current lines compared with zones 5, 6 and 7. Therefore, the temperature rise in the latter regions was anticipated to be lower than the temperature rise in zones 1, 2, and 3.

3.3 Quench Initiation and Normal-Zone Propagation

The critical current measurements were followed by a set of experiments in which at a given operating temperature, $T_{op}=60$ K, a transport current, I_t , was introduced in the tape which was then quenched by pulsing the stainless steel heater, attached to the center of the tape. A 12 W pulse lasting 0.5 s was used for triggering the quench. The transport current was cut off when the peak temperature in the tape reached ~ 300 K. In earlier experiments, for peak temperatures in excess of 400 K, the quench behavior was irreproducible, therefore the peak temperatures in the sample were kept under 400 K.

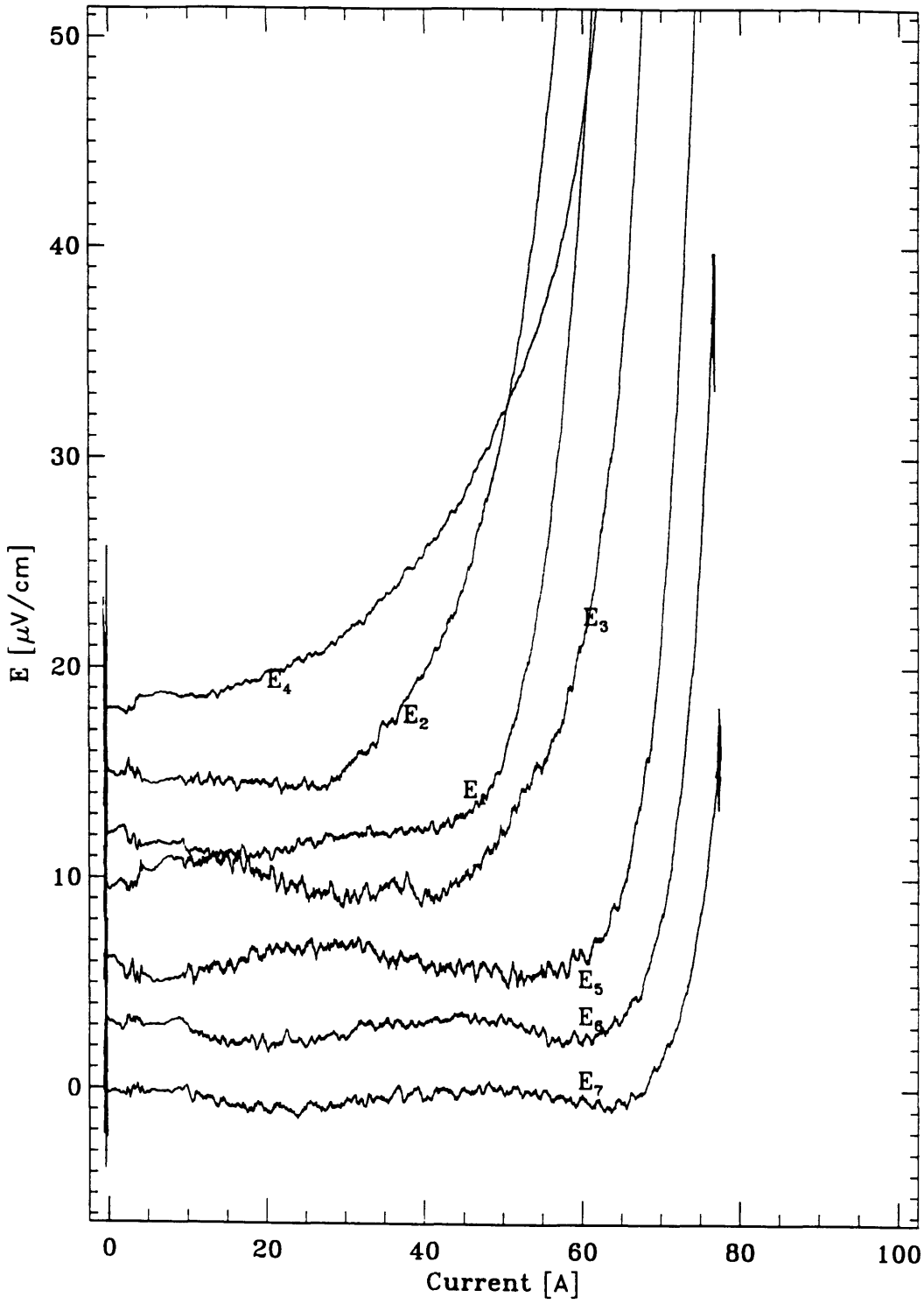


Figure 3.3: E - field traces for the seven zones at $T_{op} = 60$ K.

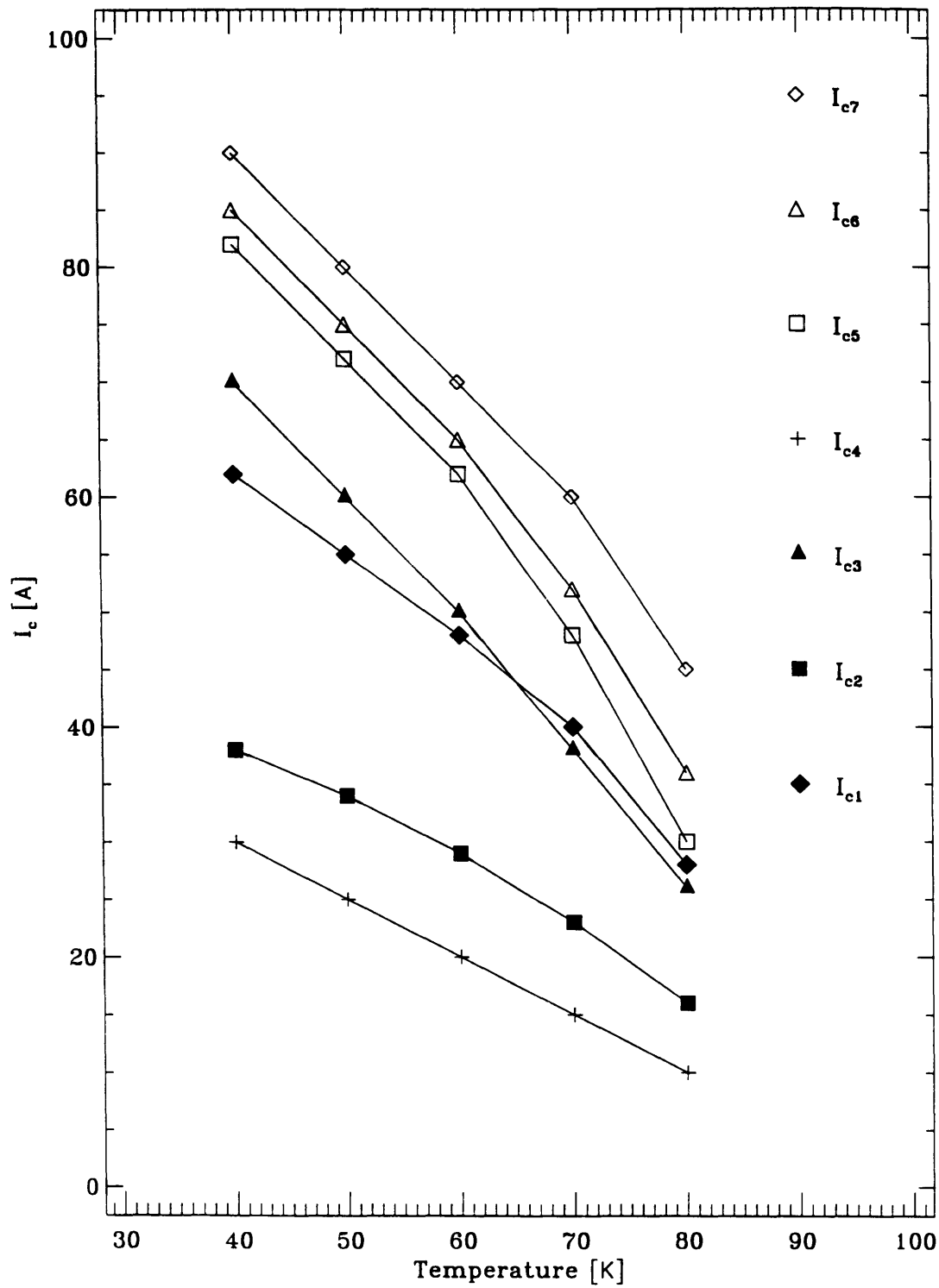


Figure 3.4 $I_c(T)$ for seven zones with $E_c = 1 \mu\text{V}$ criterion.

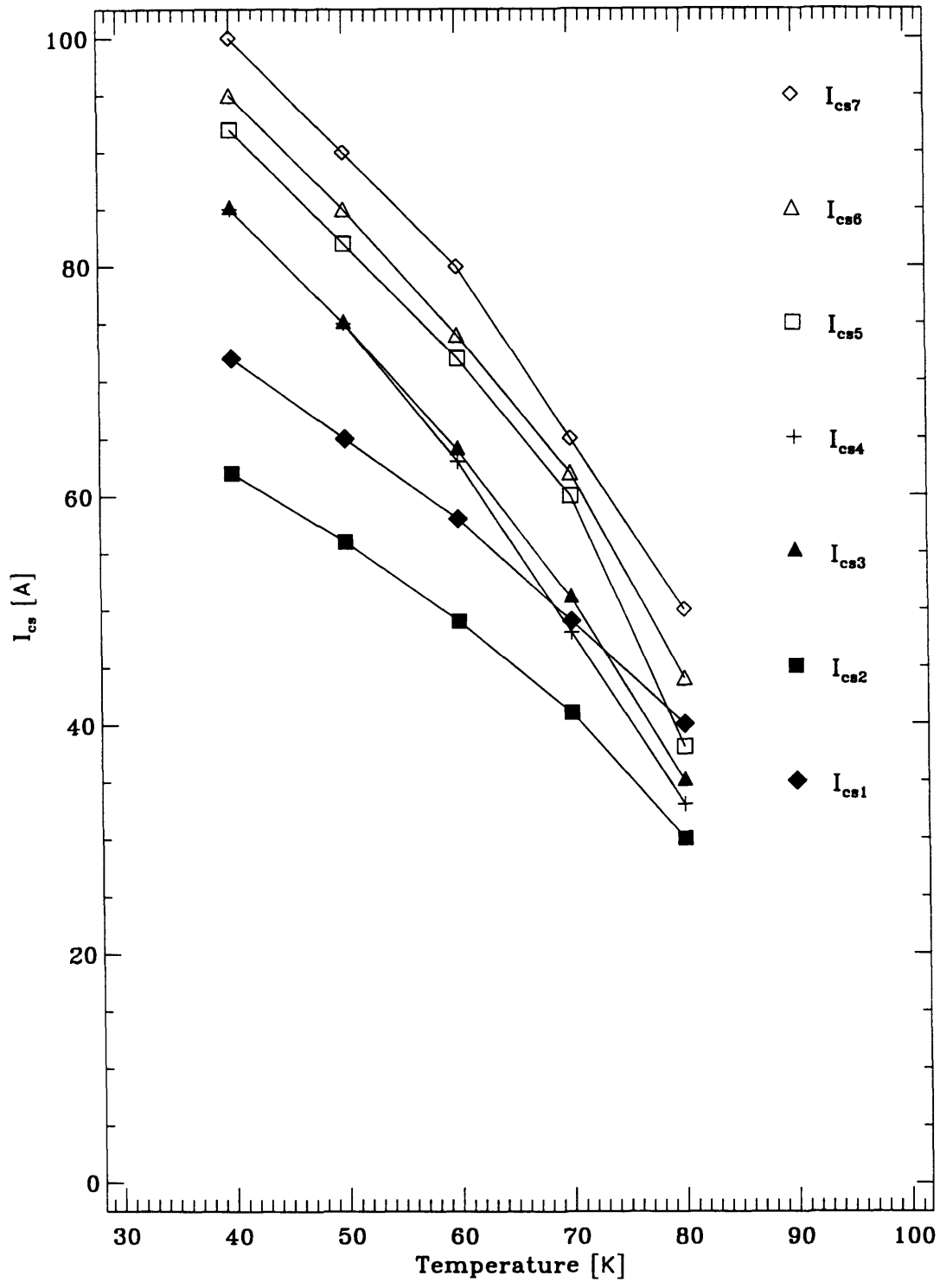


Figure 3.5: $I_{cs}(T)$ for seven zones with $E_c = 25 \mu\text{V}$ criterion.

3.4 Temperature Profiles

The measured temperature profiles at $I_{op} = 55$ A are shown in Figure 3.6. The regions closest to the current lead anchors (regions 1 and 8) show the smallest temperature rise since the quench is initiated at the center of the tape which is the farthest from these regions. The initial temperature rise occurs in region 4 because of the heater pulse. T_4 and T_5 , attached in region 4, show the initial temperature rise of this region. Figure 3.7 shows a 3-D plot of the quench with location, z , and time, t , as the independent variables and temperature, $T(z,t)$ as the dependent variable.

The decay in the temperatures occur because at $t = 16$ s the power supply is shut off. T_1 and T_8 decay faster than the other thermocouples because they are located closest to the current lead anchors which are fixed at $T_{op} = 60$ K. The peak temperature occurs in region 2 (T_2). Figure 3.5 shows that the critical current for this region is lower than the other regions. Thus the temperature distribution is related to the critical current distribution. In general, regions which show degraded critical currents will have higher temperatures during a quench as compared with regions that have high $I_c(T)$ values.

3.5 Verification of Temperature Measurements

For each region of the sample, both the temperature and the voltage were monitored. Voltage measurement on LTS and recently on HTS have been performed in prior research. To verify the validity of the measured temperatures, voltages for the zone were computed using the temperature traces for the regions. The following relationships were used to compute the voltages from the temperatures.

$$V_j(t) = 0 \quad T_{op} \leq T_j \leq T_c \quad (3.1 a)$$

$$= \frac{\rho_m(T_j)}{A_m} I_t \quad T_{cs_j} \leq T_j \leq T_c \quad (3.1 b)$$

$$= \frac{\rho_m(T_j)}{A_m} [I_t - I_{cs_j}(T_j)] \quad T_j \geq T_c \quad (3.1 c)$$

where V_j and T_j are the voltage and temperatures of the j^{th} zone of the sample. T_{csj} and I_{csj} are the critical sharing temperature and critical sharing current, as explained in Section 3.2, and T_{op} and T_c are the operating temperature and critical temperature respectively.

Figure 3.8 shows the measured (solid) and the computed (dotted) voltages of the seven zones. As expected, each computed voltage generally displays a delay in comparison with the corresponding measured voltage. This delay comes about because each temperature is measured at a specific location within a zone whereas the corresponding voltage is measured over a given zone. A positive measured voltage appears as soon as there is a quench anywhere along the zone. However a thermocouple in this zone shows a temperature rise only when the location of the thermocouple experiences a temperature rise. Thus voltage taps over a zone pick up a quench anywhere along the zone, whereas thermocouples pick up a temperature rise at their mount locations. The computed voltages and the measured voltages converge when the entire zones are normal.

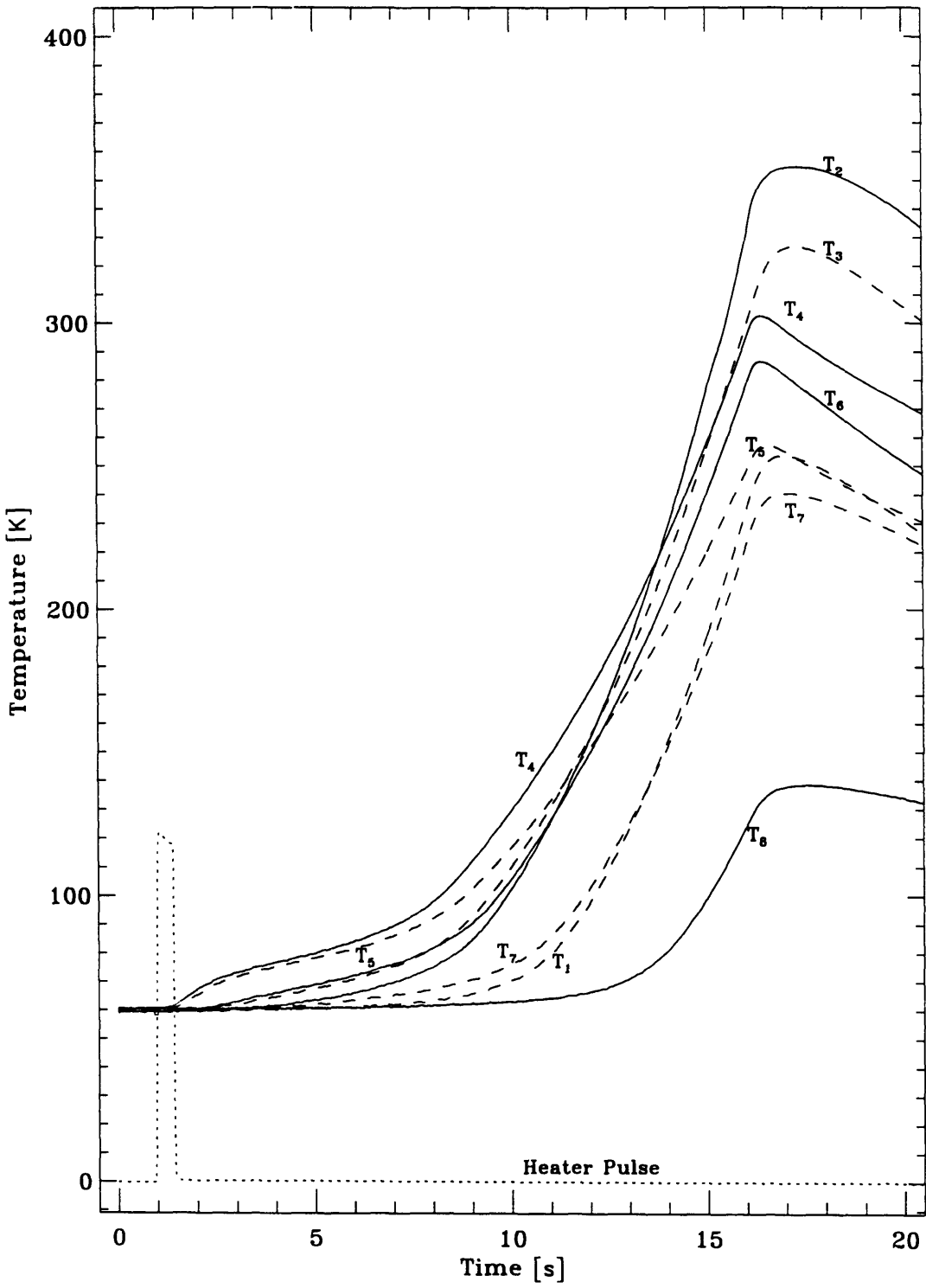


Figure 3.6: $T(t)$ traces during quenching for $I_t = 55$ A and $T_{op} = 60$ K

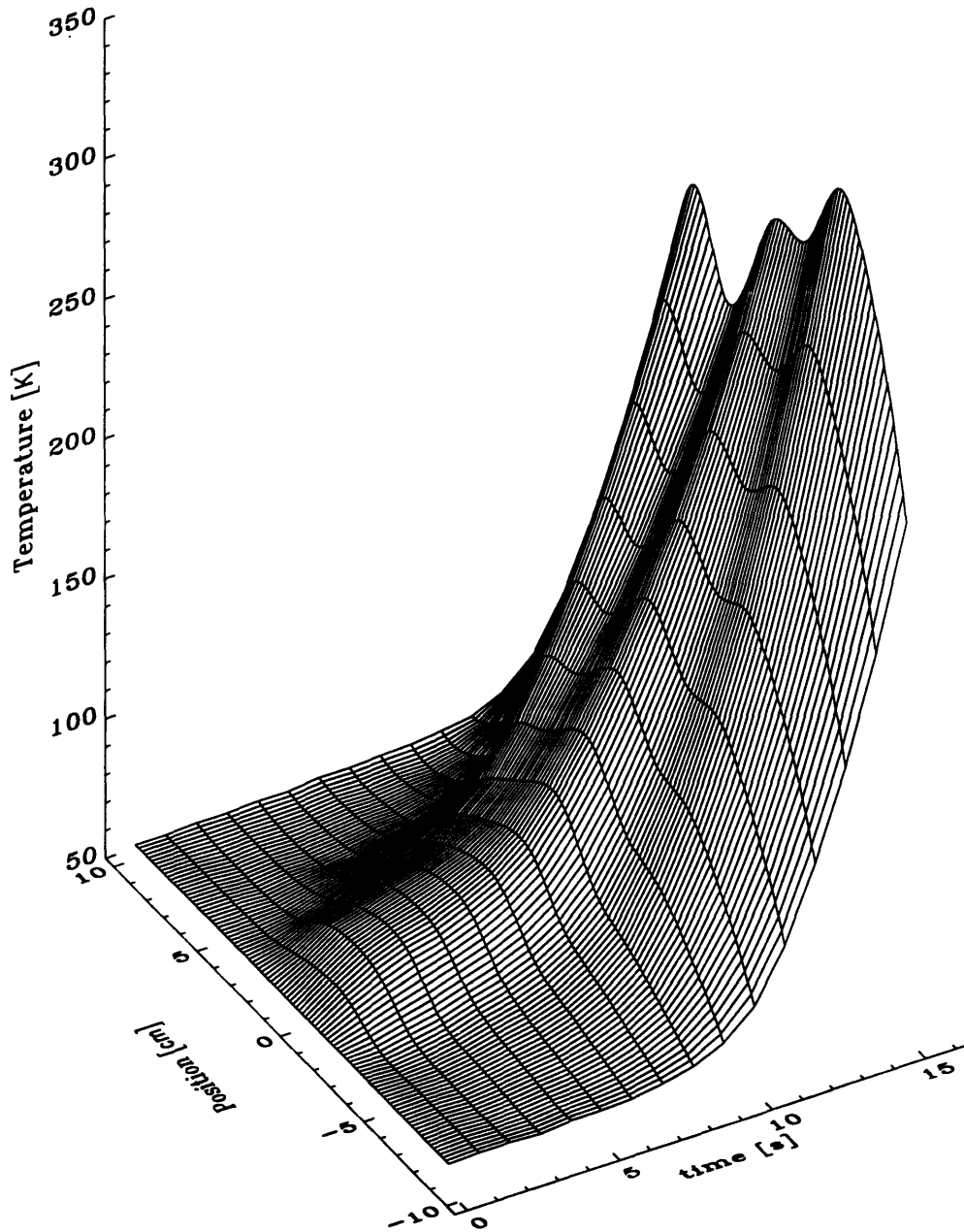


Figure 3.7: $T(z,t)$ traces during quenching for $I_t = 55$ A and $T_{op} = 60$ K.

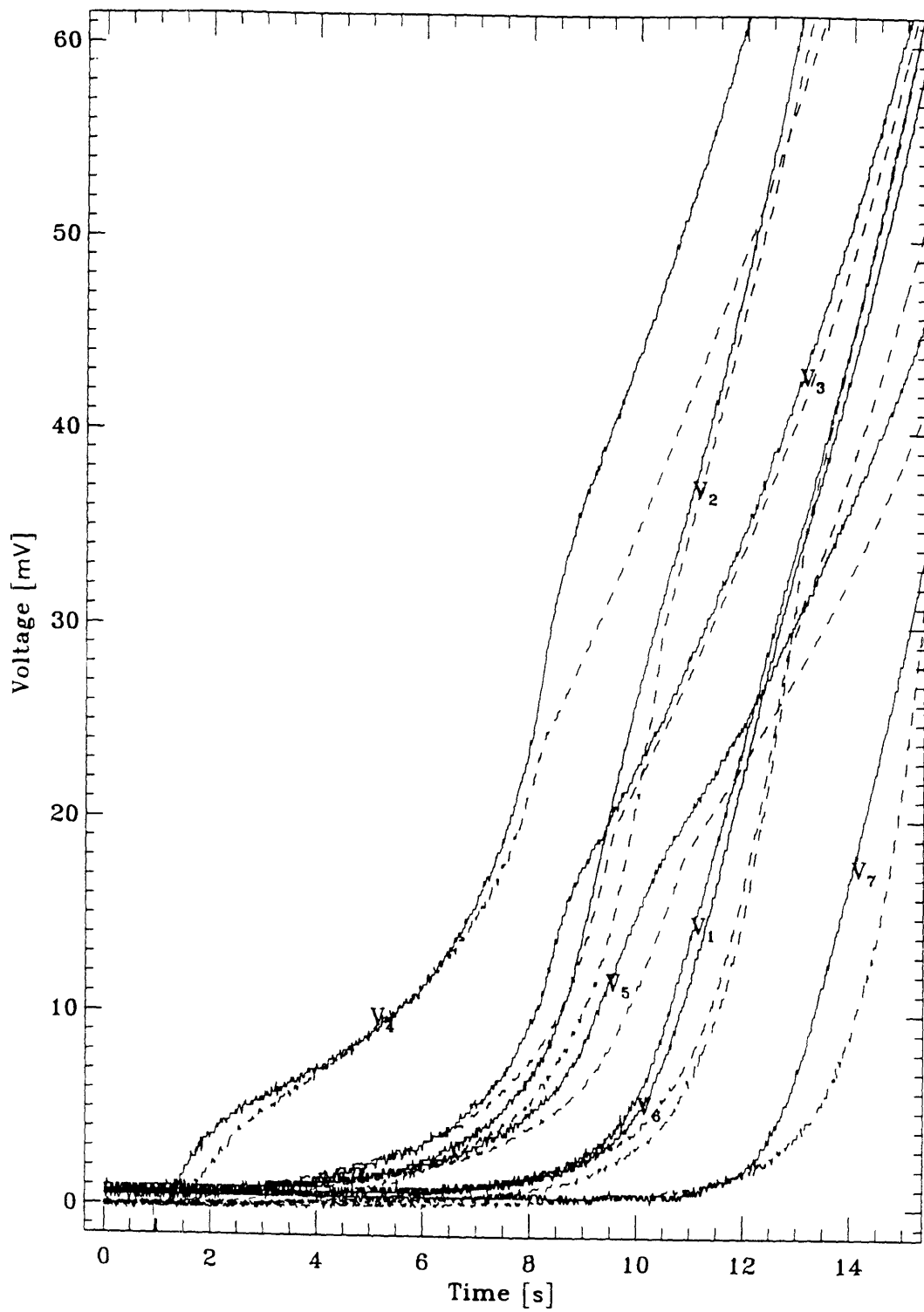


Figure 3.8: $V(t)$ traces during quenching for $I_t = 55$ A and $T_{op} = 60$ K. Solid lines are measured; dotted lines are computed from the temperature traces shown in Figure 3.6.

4 Computer Simulation of Quenching

4.1 Simulation Algorithm

The quenching process for a superconducting tape is governed by a 1-D nonlinear partial differential equation (PDE) as given by Equation 2.1. Since this equation cannot be solved analytically, it must be discretized and solved numerically. The computer code used to solve for the spatial and temporal temperature distribution of HTS tapes is described below.

The first step in solving the nonlinear PDE is spatial discretization. The 300 mm tape is discretized in 10000 differential elements, each with a spatially uniform temperature. Next, an operating temperature, spatially uniform initially, is used to evaluate the material properties thermal conductivity, specific heat, and electrical resistivity. The Joule heating is calculated for each element from Equation 2.5. The transport current remains constant throughout the quench simulation. A finite difference scheme, explained in the next section, is used to compute the temperature profile for each subsequent time step. This new temperature profile is then used to update the material properties. This scheme is repeated for the duration of the quench.

4.2 Finite Difference Method and Stability

The 1-D nonlinear partial differential equation is a parabolic PDE that is numerically solved with the

Crank-Nicolson method [5]. The strength of the Crank-Nicolson method lies in its second-order accuracy in both time and space, i.e., $O[(\Delta t)^2, (\Delta x)^2]$. For the diffusion equation as given by Equation 2.1, the following notation is used in the discretization scheme.

$$T(z,t) = T(i\Delta z, n\Delta t) \equiv T_i^n \quad (4.1)$$

Using the above notation, the finite difference representation of Equation 2.1 is given by

$$\begin{aligned} (C_{cd})_i \frac{T_i^{n+1} - T_i^n}{\Delta t} = & \frac{1}{2} \left[k_{i-1/2} \frac{T_{i-1}^{n+1} - T_i^{n+1}}{(\Delta z)^2} + k_{i+1/2} \frac{T_{i-1}^{n+1} - T_i^{n+1}}{(\Delta z)^2} \right] \\ & + \frac{1}{2} \left[k_{i-1/2} \frac{T_{i-1}^n - T_i^n}{(\Delta z)^2} + k_{i+1/2} \frac{T_{i-1}^n - T_i^n}{(\Delta z)^2} \right] + g_i^n \end{aligned} \quad (4.2)$$

where

$$k_{i\pm 1/2} = \frac{k_i^n + k_{i\pm 1}^n}{2} \quad (4.3)$$

For prescribed boundary temperatures $T(z=0)=T(z=L)=T_{op}$, at each time level, n , Equation 4.2 results in $M-2$ simultaneous algebraic equations with $M-2$ unknowns. M is the total number of differential elements used to discretize the tape ($M=10000$ for the simulation presented here). The Tri-Diagonal Matrix Algorithm is used to solve the algebraic equations.

The Crank-Nicolson method is unconditionally stable. The only restriction is that for a chosen value of

$$r = \frac{\alpha \Delta t}{(\Delta z)^2} \quad (4.4)$$

and given values of α and Δx , the value of the time step Δt is constrained by Equation 4.4.

4.3 Comparison of Results, Simulation and Experiment

As explained in Section 3.3, a set of measurements was performed in which at a given operating temperature, $T_{op}=60$ K, and a transport current, $I_t=55$ A, a quench was initiated in the HTS tape with a pulse current in the heater, attached at the center of the tape. In this section, the spatial temperature distribution of the quenching tape computed by simulation, is compared with that obtained in the experiment. Simulation is performed first with the measured nonuniform critical current distribution (see Section 3.2) incorporated. Next, it is performed with the current distribution assumed uniform.

4.3.1 Simulation with Nonuniform Critical Current Distribution

Figure 4.1 shows simulated profiles (dotted lines) that agree well with experimental temperature profiles (solid lines). Here the measured nonuniform critical current distribution is incorporated in the simulation. The first temperature profile, $t=0$ s, shows a uniform operating temperature, $T_{op} = 60$ K, across the entire length of the sample. In the next two profiles, $t= 2$ s, and $t=4$ s, the temperature rise

is dominant in the region of the heater pulse, as shown by a rise in T_5 and T_6 . For these profiles, T_1 and T_8 , both farthest from the heater, remain at the operating temperature. As the quench zone grows, the temperature of the zones adjacent to the heater also increases. The Joule heating produced for zones that have higher critical current profiles, i.e., zones 6, 7, and 8, is smaller than the Joule heating produced in zones with lower critical currents, i.e., zones 1, 2, and 3. This nonuniform Joule heating results in skewed temperature profiles with a higher temperature rise in zones with lower critical currents.

4.3.2 Simulation with Uniform Critical Current Distribution

Figure 4.2 shows the temperature profiles for the first 14 seconds of a quench at $T_{op} = 60$ K, and $I_t = 55$ A. The profiles are 2 seconds apart. The dotted profiles are simulated with a uniform critical current distribution. Since the critical current is uniform, the temperature profiles are spatially symmetric. The experimental profiles, given by diamond data points connected by solid lines, however, are asymmetric.

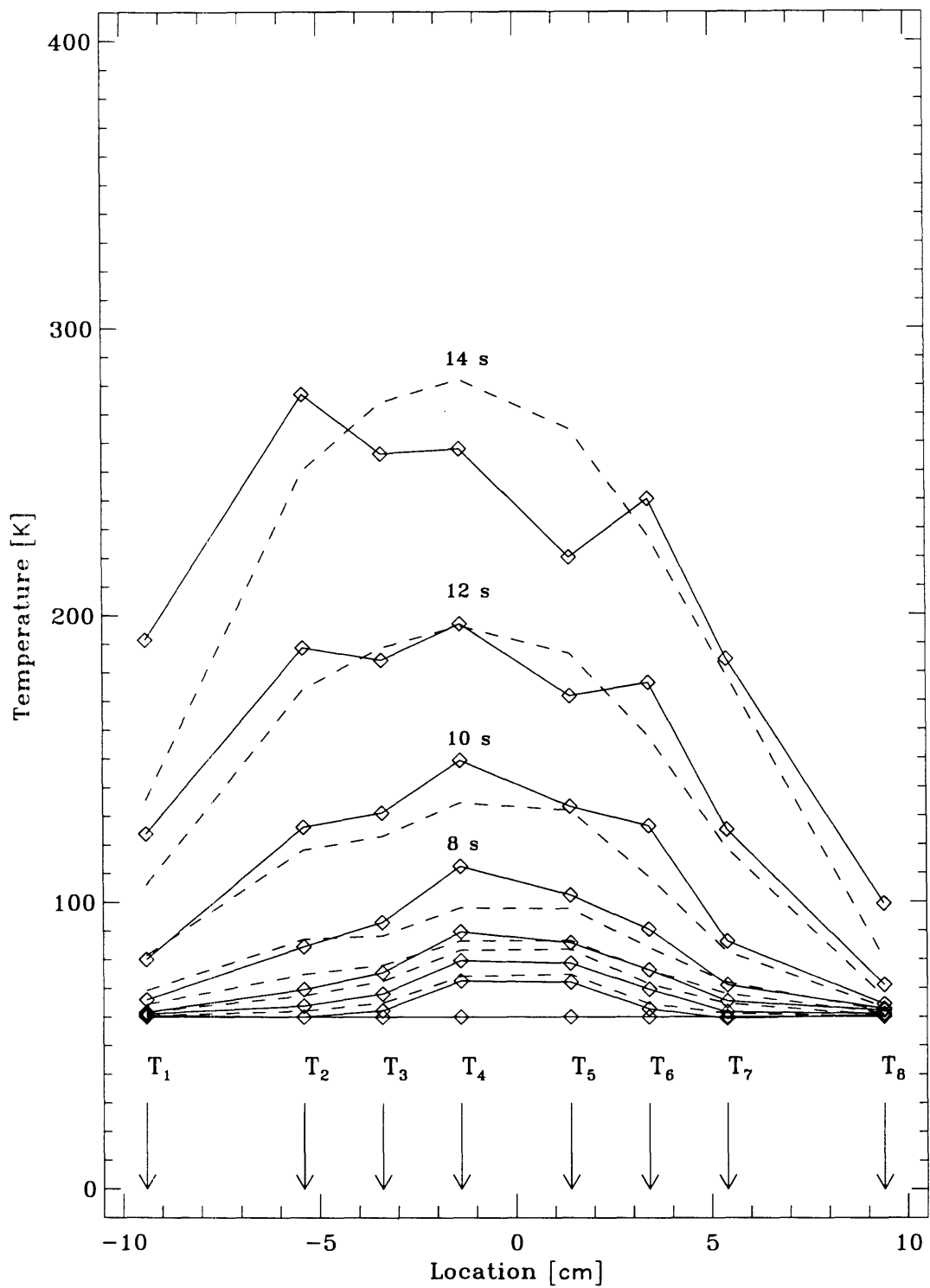


Figure 4.1: $T(z,t)$ profiles during quenching for $I_t = 55$ A and $T_{op} = 60$ K. Dotted lines are simulated profiles with nonuniform critical currents across the tape.

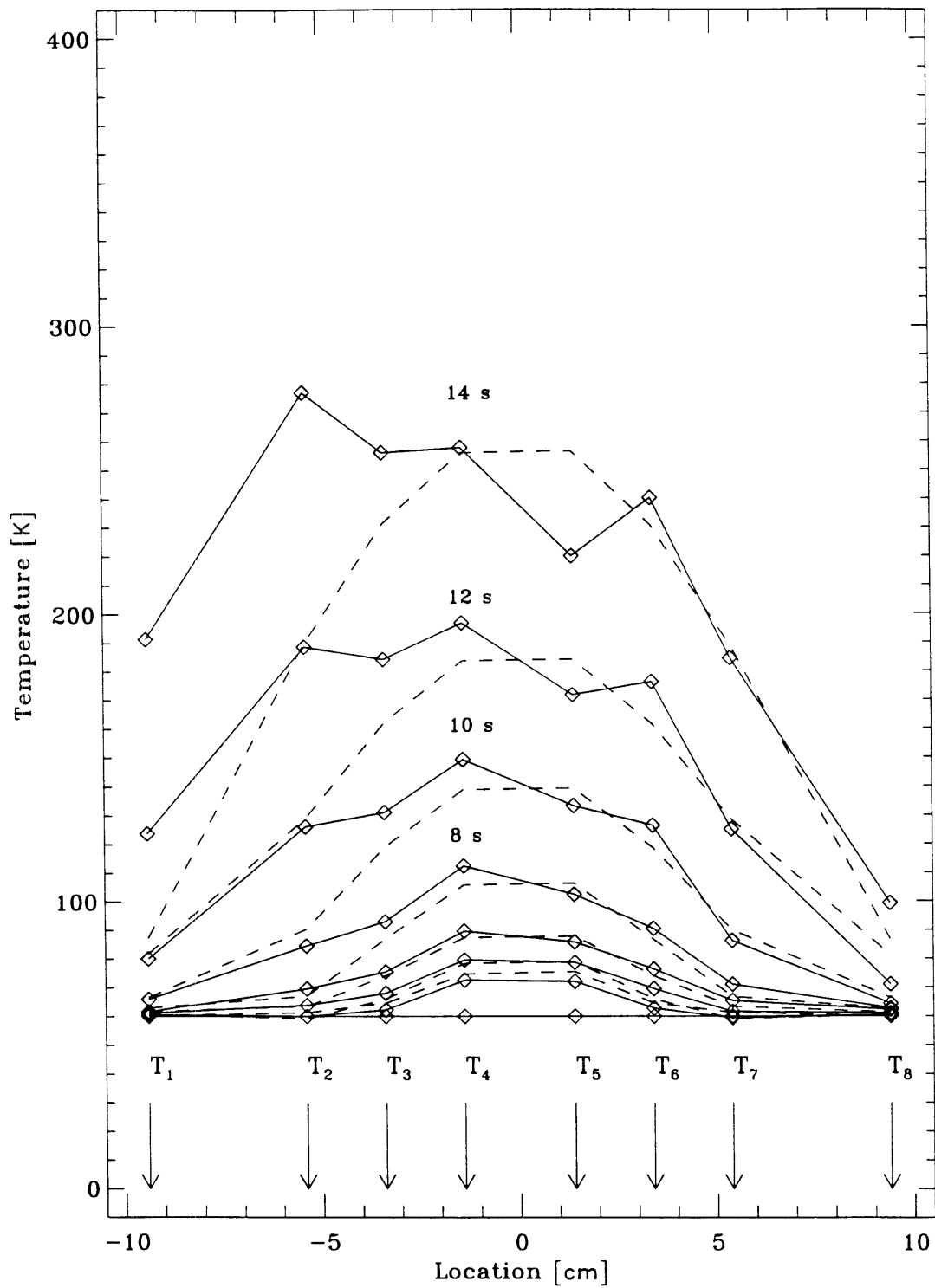


Figure 4.2: $T(z,t)$ profiles during quenching for $I_t = 55$ A and $T_{op} = 60$ K. Dotted lines are simulated profiles with uniform critical current assumed across the entire tape.

4.4 Limitations of Simulation Code

The analytical temperature profiles are based on Equation 2.6 that assumes an adiabatic condition. The excellent agreement between the experimental and the analytical temperature profiles in the beginning of the quench process, followed by a slight disagreement at later times, suggests that the adiabatic condition is not maintained at all times. Although convective cooling is negligible in the experiment, conduction is possible from contact points between the holder insulation and the sample. Furthermore, at high temperatures, radiation effects are significant. The radiation heat transfer coefficient, h_r , between the environment temperature of 60 K and a sample temperature of 400 K is 4.3 W/m²K. Thus, in modeling the behavior of HTS tapes the adiabatic assumption may be violated as the tapes are heated to high temperatures.

A second source of error in modeling the quench behavior of the tapes is the heater pulse. The simulation ignores the mass of the stainless steel heater and the thermal resistance between the heater and the sample. At $t=2$ s in Figure 4.1, the experimental and simulated temperature rise caused by the heater pulse show an excellent agreement. However, for later times, the experimental profiles show a greater heating than the simulated profiles. This disagreement is most likely caused by a thermal lag between the heater and the tape.

A final source of error in the simulation is the assumption that the temperature at each end of the sample remains at the operating temperature, T_{op} . The dotted simulation temperature profile at $t=14$ s in Figure 4.1 shows temperature at the extremities, T_1 and T_8 that are lower than the observed temperatures at these locations. As the quench proceeds, at later times, the assumption that the current leads are at the operating temperature, T_{op} , may no longer be valid. In this case, resistive heating at the current leads can result in temperatures at the extremities of the HTS tape that are higher than those predicted.

5 Conclusions

A thorough understanding of quench behavior is essential for proper design in applications of HTS technology such as magnets, generators, and DC transmission systems. The main focus of this research has been on the experimental and analytical investigation of the thermal and electrical behavior of HTS tapes. For the samples tested in this research, a nonuniform critical current distribution is observed. The nonuniformity is most likely inherent in the manufacturing process of the HTS tapes. The nonuniformity in the critical current results in asymmetric temperature profiles with the area of lowest critical currents (weak spots) showing the largest temperature rise. This weak -spot effect and quench protection of HTS magnets are discussed in the following sections.

5.1 Effect of Weak-Spots in Conductor

From the $T(z,t)$ profiles in Figure 4.1, when the heating is confined to the heater zone and its immediate neighbors, the profiles are symmetric with respect to the heater location. For later times when the heating spreads over the entire sample, the weak-spot, i.e., zone 2, experiences the largest dissipation, hence the fastest temperature rise. This results in an asymmetric temperature profile at later times.

Quench propagation is inherently slow in high- T_c conductors as compared with that in low- T_c conductors [6,7]. This means that HTS magnets are not self-protecting and need protection mechanisms to ensure safe quenches. The slow quench process in HTS tapes is exacerbated by the presence of weak -

spots. Quenches that are not induced by a heater are likely to occur at the weak spots. The localization of such quenches in HTS magnets will result in excessive heating and possible melt down at the weak spot.

5.2 Protection Schemes for HTS magnets

Multicoil superconducting systems for Nuclear Magnetic Resonance (NMR) application are now commercially available up to the 750 MHz range. In general, such magnet systems consist of concentric outer NbTi coils and inner Nb₃Sn coils. The coils, connected in series, are shunted for limiting the voltage rise during quench. If the outer NbTi coils quench before the Nb₃Sn coils, large induced currents in the Nb₃Sn coils can result in Lorentz stresses in excess of the magnet's yield strength. To prevent irreversible damage to the inner coils, stainless steel heaters, mounted on the outermost layer of these coils, are triggered when the NbTi coils quench. Thus, the Nb₃Sn coils are forced to quench and current build up in these coils is prevented.

The tolerance of HTS magnets to background field make them ideal for use in Giga-Hertz class NMR magnet systems. A typical 1 GHz magnet will consist of an HTS magnet as the innermost coil. Unfortunately, unlike the Nb₃Sn coils, heaters will not be effective in triggering a quench in the HTS coils. Heater quenches may even result in destroying HTS magnets instead of protecting them because, as seen in the present research, the highest temperature rise may occur at location other than the heater location.

The most feasible protection for HTS coils will involve mechanisms which will prevent induced

quenches in the HTS coil. A protection scheme that consists of low resistance, high mass shunt resistors coupled with diodes may be used to prevent current build up in HTS coils. The diodes prevent such current build up until their break voltage is exceeded, at which point current will begin to increase in the HTS coil. With a low resistance shunt, a significant fraction of the energy will be dissipated by the shunt resistor, thus protecting the HTS coils from large Lorentz stress and excessive heating.

References

- [1] P. Haldar, J. G. Hoehn Jr., Y. Iwasa, H. Lim and M. Yunus, "Development of Bi-2223 HTS high field coils and magnets," *IEEE Trans. Appl. Supercond.* (1995).
- [2] P. Haldar, J. G. Hoehn Jr., L.R. Motowildo, U. Balachandran, Y. Iwasa, M. Yunus, "Recent development in processing HTS silver-clad Bi2223 tapes, coils and test magnets," *Proc. of the 6th International Symposium on Superconductivity, Hiroshima, Japan* (1993).
- [3] R.H. Bellis and Y. Iwasa, "Quench propagation in high T_c superconductors," *Cryogenics* **34**, 129 (1994).
- [4] Yukikazu Iwasa and Mamoon I. Yunus, "Spatial and temporal temperature and voltage signals of a silver-sheathed BSCCO tape undergoing a quench: Experimental and analytical results," *Proc. of the European Conf. on Applied Superconductivity* (1995).
- [5] M. Necati Ozisik, *Finite Difference Methods in Heat Transfer*. (CRC Press, Inc., Boca Raton, Florida, 1994).
- [6] Yukikazu Iwasa, *Case Studies in Superconducting Magnets*. (Plenum Press, New York, 1994).
- [7] Y. Iwasa, H. Lim, and M.I. Yunus, "Stability and Quenching in high-temperature superconductors," *IEEE Trans. Appl. Supercond.* (1995).

Appendix A

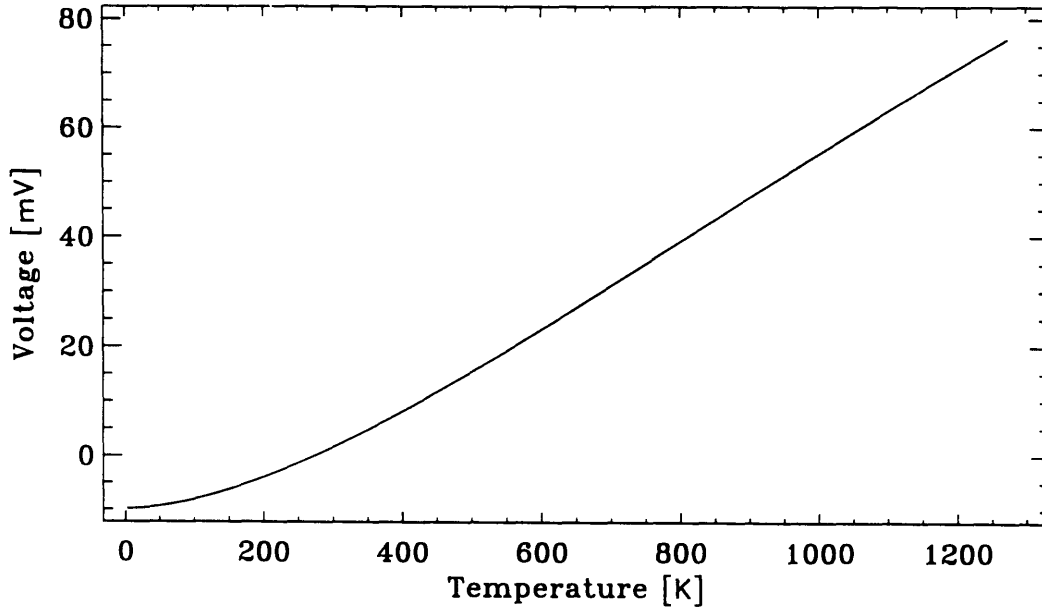


Figure A-1: Thermoelectric voltage versus temperature for a Type E thermocouple.

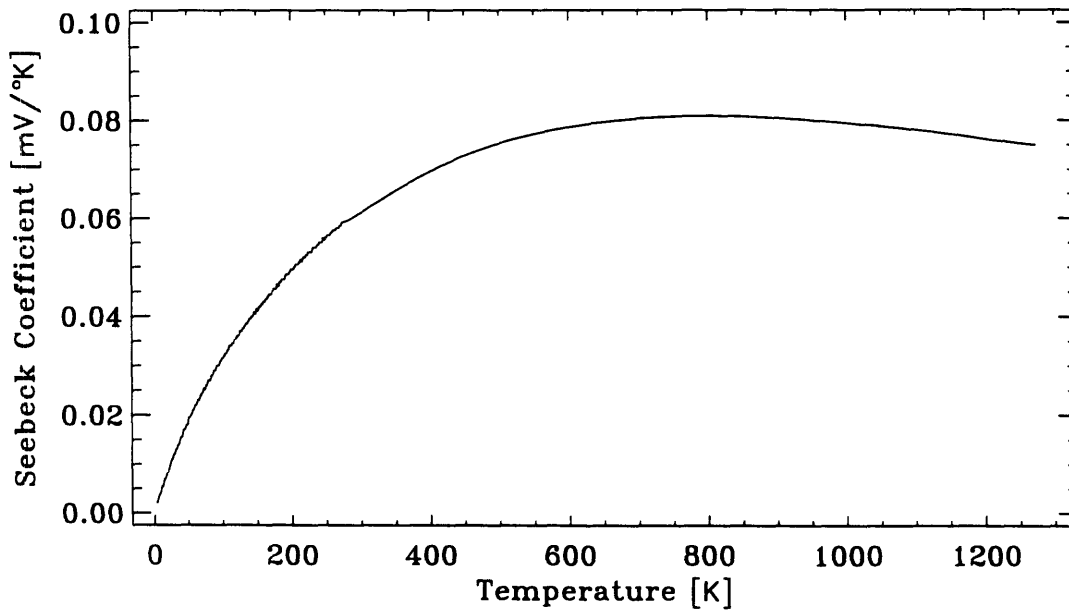


Figure A-2: Seebeck Coefficient versus temperature for a Type E thermocouple.